Spectral behavior of high-power Compton free-electron lasers. II. Effect of filtering and tapering on sideband generation

D. Iracane and P. Chaix
Commissariat à l'Energie Atomique, Centre d'Etudes de Bruyères-le-Châtel, Service de Physique et Technique Nucléaire, Boîte Postale 12, 91680, Bruyères-le-Châtel, France

H. Delbarre
Université des Sciences et Technologies de Lille, Laboratoire de Spectroscopie Hertzienne, 59655, Villeneuve d'Asq, France
(Received 22 April 1993)

We show via a numerical study of the asymptotic spectral behavior of filtered and tapered free-electron-laser (FEL) oscillators that tapering must in general be assisted by filtering to prevent spectral broadening. To interpret these results, we present a theoretical analysis of the sideband instability, including the transient regime. For long amplifiers, an analysis of trapped particles appears to be relevant. This is not the case for an FEL oscillator where the standard "deeply-trapped-electrons" and "exponential-regime" assumptions are most often irrelevant. Moreover, spectral broadening is not related in a simple way to a sideband inhibition, due to the multiplicity of nonlinear mechanisms involved in FEL dynamics.

PACS number(s): 41.60.Cr, 52.35.Mw, 52.35.Ra

I. INTRODUCTION

It is expected, on both theoretical and numerical grounds, that the sideband instability in high-power free-electron lasers (FEL's) is the first step of a broadening of the emitted spectrum, due to the diffusion of the electrons in their phase space (preceding paper I). More than an academic investigation of the sideband mechanism, the present paper is an attempt to understand the transient regime responsible for spectral broadening. This work will show that the realistic FEL spectral behavior is very intricate and cannot be understood by simply defining the sideband generation as a trapping instability [1].

Many publications are devoted to the sideband generation, associated in most cases with complementary mechanisms such as filtering or tapering (lowering of the ponderomotive bucket in the electron phase space). Tapering has often been said to slow sideband generation [2,3], or even to inhibit it [4]. This can be due to two effects: first the distortion of the orbit when the resonant electron is slowed down at a rate comparable with the synchrotron motion. Second, for a tapered wiggler, the bucket is smaller so that a smaller number of electrons can couple with the sidebands.

However, the concept of tapering is meaningful only with a monochromatic laser field. Indeed, many publications [5,6] emphasize that a small amount of sideband can detrap electrons from the ponderomotive bucket, which can make the tapering inefficient.

Now, the effect of filtering is not trivial. On one hand, following paper I, one expects that the extraction efficiency is decreased by filtering. Such a result has been stated in many publications, either for nontapered wigglers [7] or tapered ones [8,9]. On the other hand, the tapering scheme may be more efficient for a filtered FEL, so that one can expect to enhance the efficiency; this prediction has also been observed [10]. Experimental data also corroborate these statements. Indeed, in Ref. [11], three different tapered wigglers were used and spectral broadening was controlled by detuning the optical cavity [7]; it is claimed that, for some cavity detuning, broad-spectrum regimes are observed whatever the tapering. For a shorter optical cavity, the spectrum gets narrow and the efficiency is improved [11] (depleted [7]) for tapered (nontapered) wigglers. For some intermediate detuning, the plot of the efficiency versus time, within a single macropulse, exhibits a very subtle behavior since the tapering begins to increase the efficiency, but then sidebands appear and the efficiency collapses.

Considering parameters close to those of the experiment of Ref. [7], but in the continuous-beam limit, we exhibited, in paper I, a strong spectral broadening phenomenon, related to some randomization of the electron phase space. In such a case, tapering becomes inefficient due to the very complicated phase-space structure [12]. Note that this second regime is characteristic of high-power FEL's and requires high electronic currents and long interaction times. This is why the broad spectrum regime was only observed in few experiments, up to now [7]. Therefore, there is clearly a threshold in the physical experimental parameters that controls which asymptotic regime will occur.

Experimental evidence shows that tapering is not expected to eliminate the sidebands, but only to delay them. Then, trying to understand the variety of FEL behaviors depending on the rate of tapering, it is necessary to use a second independent parameter that governs the spectral regime. The simplest one is a filter. For theoretical purposes, a filter provides a better control parameter than the electronic current, the pulse length, or the optical cavity detuning, since it does not change the coupling constants of the problem. Furthermore, it can be easily

implemented in our numerical simulations working on a Fourier expansion of the laser field.

We therefore consider the spectral behavior of a high-current FEL oscillator, with parabolic tapering and a filtering device. The starting point of our analysis is a numerical investigation versus the tapering amplitude $\Delta B/B$ and the filter width (Sec. II). This two-parameter set of numerical experiments shows a transition between narrow and broad spectra. To understand this transition, we first present an analysis of the sideband instability and then consider the relation between sideband inhibition (by tapering and/or filtering) and spectral broadening.

To investigate the effects of sideband generation, numerical simulations are required and widely used [2–4,6,8–10]. Other studies are devoted to the interpretation of the sideband instability from a basic point of view [5,13–18]. As an academic starting point, most of these papers assume that electrons are initially bunched on the orbits of the ponderomotive well. Even if they shed some light on the mechanisms of the sideband instability, one should question their reliability for a realistic description. Therefore, it is necessary to address the connection between the academic approach and full numerical simulations.

As a first step of our analysis of the sideband instability, we provide a generalization of the standard sideband model, starting with a monochromatic laser and an electron distribution in equilibrium in the ponderomotive wells (Secs. III and IV), but not assuming an exponential growth of the instability. This allows us to study the transient regime. We will show that, for most oscillator experiments, the transient regime actually lasts longer than the wiggler length, which then makes irrelevant the usual asymptotic exponential gain calculations.

As a second step, we implement the time-dependent perturbation theory presented in Sec. III by using an adiabatic assumption. Within an investigation of the sideband generation in a strongly tapered long amplifier (Sec. V), we obtain (i) an expected result about the importance of the trapping ratio and (ii) a more surprising outcome about the adiabaticity of the trapped particle motion. This allows us to interpret the sideband depletion in a strong tapered amplifier. Nevertheless, sidebands appear to be inhibited mainly because an amplifier is a finite-time experiment: the same tapering rate within a resonator experiment would lead to a quite different spectral behavior.

As a third step, we consider the system with more realistic nonbunched nonequilibrium initial conditions. Low-noise numerical simulations allow us to test whether or not the sideband will grow in a given tapered and filtered system. Then we come back to the problem of the evolution over a large number of round-trips for a tapered FEL oscillator assisted by filtering (Sec. VI). In particular, we show that the sideband instability in a filtered system does not necessarily lead to a broad spectrum (that is a spectrum as wide as the filter): mode competition between fundamental and sideband modes can actually lead to a spectrum much narrower than the filter.

As mentioned in paper I, the spectral dynamics can be studied using a one-dimensional (1D) model. For that purpose, we assume that the laser electric field $\mathcal{E}_n$ and electron density are proportional to Gaussian radial profiles $S(r)$ and $T(r)$. This leads to the following set of equations where we recognize the standard 1D formulation [1,19,20]. For analytical investigations, the Vlasov-Maxwell approach is well suited especially if we define $p=\gamma^2$, where γ is the electron kinetic energy normalized to its rest energy. The electronic motion can then be put easily under a Hamiltonian form with conjugate variables $(\psi,p=\gamma^2)$ and with the transformed density $h(z,\psi,p)=g(z,\psi,\sqrt{p})/\sqrt{p}$. We define a reference wave number k_L and recall the equations of the model:

$$A_L=\frac{mc}{e}\mathrm{Re}\sum_{n\,(\ll N)}\frac{\mathcal{E}_n(z)}{k_n}e^{ik_n(z-ct)}\,, \tag{1}$$

$$id_z\mathcal{E}_n=\mu_0e^2ca_w\mathcal{H}_1\frac{1}{\pi r_e^2}\times\int_1^{+\infty}\frac{dp}{2\sqrt{p}}\frac{1}{2\pi N}\times\int_0^{2\pi N}d\psi\,h(z,\psi,p)\exp(-i\psi_n)\,, \tag{2a}$$

with

$$k_n=\left[1+\frac{n}{N}\right]k_L\,,$$

$$\psi=(k_L+k_w)z-k_Lct\,, \tag{2b}$$

$$\psi_n=\left[1+\frac{n}{N}\right]\psi-\frac{n}{N}k_wz\,,$$

$$[\partial_z+(\partial_pH)\partial_\psi-(\partial_\psi H)\partial_p]h(z,\psi,p)=0\,, \tag{3a}$$

$$\partial_pH=k_w-k_L(1+a_w^2/2)/2p\,, \tag{3b}$$

$$-\partial_\psi H=\langle ST\rangle(\pi r_L^2)^{1/2}\mathcal{H}_1a_w\mathrm{Im}\sum_{n\,(\ll N)}\mathcal{E}_n\exp(i\psi_n)\,, \tag{3c}$$

$$\frac{1}{2\pi N}\int_0^{2\pi N}d\psi\int_1^{+\infty}dp\,h(z,\psi,p)=\frac{1}{mc}\rho_e\,, \tag{4}$$

where the on-axis electric field $\mathcal{E}_n$ depends on the z coordinate, ρ_e is the number of electrons per unit of length, and r_e and r_L are the quadratic mean radius of the electron and laser beams. In the following we will consider without loss of generality that $r_e^2=2r_L^2$, which leads to $\langle ST\rangle(\pi r_L^2)^{1/2}=1/2$. The Hamiltonian H describing the electronic motion is defined by Eqs. (3b) and (3c).

II. SPECTRAL BEHAVIOR VERSUS TAPERING AND FILTERING

This section is devoted to the analysis of the spectral behavior of an FEL oscillator, which basically implies that the wiggler length and the synchrotron period have the same order of magnitude at saturation.

As a first step, let us consider a uniform wiggler (squares in Fig. 1). We know from paper I that the cou-

pling between the sideband and the fundamental modes will lead to a broad spectrum. We define a central mode at the wave number k_L of maximum linear gain. A square filter with a bandwidth $\mathcal{F}$ is used to cut off the modes of wave number k with $|k-k_L|/k_L > \mathcal{F}/2$. To analyze the effects of this filter, we define the efficiency ρ as the ratio of the extracted laser energy to the initial electron energy, the relative spectral width $\Sigma = \sqrt{\langle k^2 \rangle - \langle k \rangle^2}/k_L$, and the brightness $\mathcal{B} = \rho/\Sigma$.

On one side for large enough filters ($\mathcal{F} > 3\%$ in our case), Fig. 1(a) shows that the extracted efficiency ρ increases monotonously with $\mathcal{F}$, while Fig. 1(b) shows that the brightness $\mathcal{B}$ reaches its universal value $\mathcal{B} = \sqrt{3}/2$. This is consistent with a laser spectrum looking like a plateau truncated by the filter, and we call this the broad spectrum regime. On the other side, Fig. 1(b) shows a sharp transition toward high values of $\mathcal{B}$ for $\mathcal{F} < 3\%$: the sideband has been suppressed, and the laser spectrum is much narrower than the filter. This case will be referred to hereafter as the narrow spectrum regime.

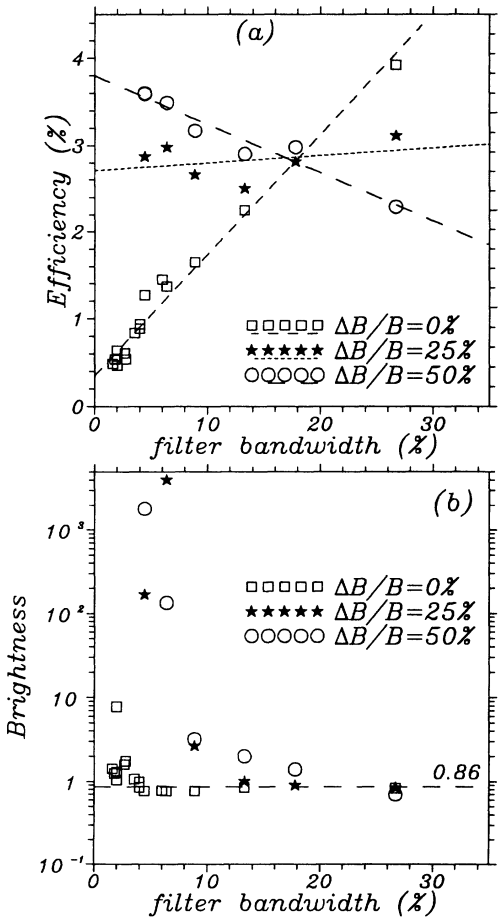

FIG. 1. Behavior of a high-power filtered FEL. (a) For a uniform wiggler, the extracted efficiency is roughly proportional to the filter width $\mathcal{F}$: the spectrum is nearly flat and merely truncated by the filter. For a strongly tapered wiggler, the efficiency versus $\mathcal{F}$ decreases because of the spectral broadening. (b) Narrow filters prevent spectral broadening, so that the asymptotic spectral width is much smaller than the filter width and the brightness $\mathcal{B}$ is large. As soon as the filter is wide enough to allow spectral broadening, the brightness is constant and equal to its universal value $\mathcal{B} = \sqrt{3}/2 \simeq 0.86$. For a tapered wiggler, the broadening is simply delayed.

The problem of determining how narrow the laser spectrum can be, once the sideband is inhibited, is under investigation and will be addressed elsewhere. As a preliminary result, it seems that the ultimate relative width is less than 10^{-4} and can be obtained with a filter bandwidth in the range of $\mathcal{F} = 1\%$ (in our case the sideband grows with a relative frequency shift of about 3%). So, by using rough gratings, it is possible to eliminate the sideband and then, by a purely dynamical effect, to get a very sharp spectrum. This result has to be validated so that FEL devices can be used for spectroscopy purposes.

As a second step, let us consider a tapered wiggler (stars and circles in Fig. 1). Simulations presented in paper I have shown that for a nonfiltered ($\mathcal{F} \to \infty$) high-power FEL, tapering becomes inefficient: it does not eliminate spectral broadening and does not increase the efficiency. A two-parameter analysis is then necessary to understand the effect of tapering for a given value of the filter. We consider a parabolic profile of the wiggler magnetic field defined by

$$B(z) = B_0 - \frac{\Delta B}{L_w^2} z^2 ,$$

where z is the longitudinal position ranging from 0 to the length of the wiggler L_W (since most of FEL oscillator wigglers are short, such a simple parametrization of the wiggler magnetic-field envelope is in general sufficient for our purpose). For each value of the magnetic field, one can define the energy of the resonant electron

$$\gamma_r^2(z) = \frac{k_L}{2k_w}\left[1 + \tfrac{1}{2}a_w^2(z)\right] . \tag{5}$$

For example, with a wiggler parameter a_w close to 0.75, a 50% variation of the magnetic field gives a 9% relative decrease for the resonant energy.

It is clear from Fig. 1(b) that the spectral behavior is affected by tapering since a larger filter bandwidth is sufficient to reach a given brightness. Nevertheless, for large enough filters, the broad-spectrum regime is reached.

The intricate consequences of filtering and tapering on the efficiency [7–11] are manifest in Fig. 1(a) where the efficiency versus filtering presents a positive (negative) slope for small (large) tapering rates. It should be noticed that maximum efficiency can be reached in two basically different ways. One can let the spectrum broaden and, following paper I, electronic diffusion enhances the efficiency, or one can filter the spectrum and use a tapered wiggler to decelerate the electrons.

The map in Fig. 2 aims at pointing out the diversity of the asymptotic regimes. The plane $(\Delta B/B, \mathcal{F})$ is divided into four regions according to the value of the brightness: black points indicate a brightness $\mathcal{B} \gg 1$ and white points indicate a brightness of the order of magnitude unity [a criterion based on the fraction of the total laser energy enclosed in a 1% spectral band around k_L leads to the same partition of the $(\Delta B/B, \mathcal{F})$ plane]. This map reveals

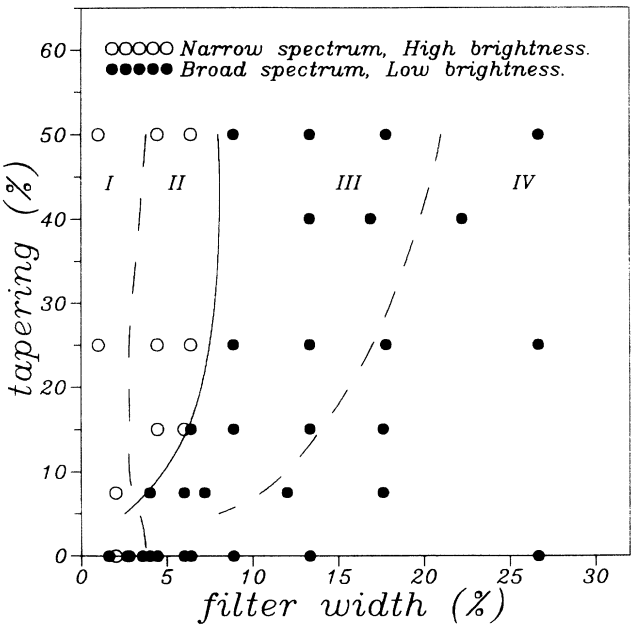

FIG. 2. Spectral behavior of a tapered and filtered system as a function of tapering amplitude $\Delta B/B$ and relative filter width $\mathcal{F}$. A sharp transition appears between broad-spectrum and narrow-spectrum regimes. In any case tapering must be assisted by filtering to prevent spectral broadening. However, tapering has an effect since it allows wider filters. See the text for a detailed description.

that the transition between the narrow- and broad-spectrum regimes depends on tapering: although tapering does not always imply a monochromatic laser field, we see that it makes it easier to avoid the sideband instability and the consecutive spectral broadening. However, it appears that tapering always needs to be assisted by filtering. Furthermore, a strong enhancement of the tapering is required to compensate for a small enlargement of the filter. Since a too strong tapering (say $\Delta B/B$ beyond 50%) also switches off the interaction, tapering cannot be used efficiently to control the spectrum of high-power FEL oscillators.

More precisely, for a narrow window (region I in Fig. 2), the sideband is clearly suppressed, so that we get a very narrow spectrum. For a large filter (region IV), tapering becomes inefficient. In that case, the sideband develops and nonlinear difference frequency generation leads to a broad spectrum with universal brightness $\mathcal{B}\cong\sqrt{3}/2$, paper I]. This implies that, even with a 50% variation of the magnetic field, we observe the same extracted efficiency and the same spectral width as for a nontapered wiggler. For realistic high-power FEL's, the broadening mechanism is strong and fast enough to complicate the phase-space structure so that it is no longer possible to define the resonant electron and its adiabatic motion induced by tapering.

Between these two extreme regimes (inhibited sideband and broad spectrum) we observe two intermediary regions. Going from region IV to region III, the brightness gets somewhat higher than the universal value: the effects of filtering begin to appear. But going from region III to region II one crosses a sharp transition line, and the spectral width drops to very small values (down to numerical resolution and in any case much smaller than the filter width).

III. SIDEBAND GROWTH FOR DEEPLY TRAPPED ELECTRONS

To get more insight in the dynamics of spectral broadening, we present an analysis of the sideband instability, including the transient regime. In fact, one usually works in the asymptotic regime by computing exponential growth rates [13]. But if we consider an oscillator, the synchrotron length at saturation is close to the wiggler length, so that the sideband exponential growth rate is not relevant, as will be seen, for instance, in Fig. 3.

We will define an equilibrium characterized by a monochromatic laser field $\mathcal{E}_0$ and a stationary electronic distribution h_0. A perturbation taking into account the coupling to new laser modes $\mathcal{E}_n$ with $n\neq 0$ makes this equilibrium unstable. An integro-differential equation will be derived for the evolution of the sidebands in the linear regime, when the initial electronic distribution h_0 is peaked at the bottom of the potential wells. This equation can be solved for all times without supposing an exponential growth. Because electrons are coupled to the laser field through its real part, the modes $\mathcal{E}_n$ and $\mathcal{E}_{-n}$ are coupled [14] and will have to be considered within the same calculation.

For a monochromatic laser field $\mathcal{E}_0(z)=|\mathcal{E}_0(z)|\exp^{-i\phi(z)}$, the force $-\partial_\psi H_0$ acting on an electron is from Eq. (3c):

$$-\partial_\psi H_0=\tfrac{1}{2}a_w\mathcal{K}_1|\mathcal{E}_0|\sin(\psi-\phi)\ , \tag{6}$$

and is therefore 2π periodic in the variable $\zeta=\psi-\phi$, which takes into account the drift due to the changing laser field. Using this variable, the dynamical equations become

$$(d_z\phi+id_z)|\mathcal{E}_0|=\mu_0 e^2 c a_w\mathcal{K}_1\int_1^{+\infty}\frac{dp}{2\sqrt{p}}\frac{1}{2\pi N}\int_0^{2\pi N}d\zeta\, h(z,\zeta,p)\exp(-i\zeta)\ , \tag{7}$$

$$[\partial_z+(\partial_p H_0)\partial_\zeta-(\partial_\zeta H_0)\partial_p]h(z,\zeta,p)=0\ , \tag{8a}$$

$$\partial_p H_0=(k_w-d_z\phi)-\tfrac{1}{2}k_L(1+a_w^2/2)/p\ , \tag{8b}$$

$$-\partial_\zeta H_0=\tfrac{1}{2}\mathcal{K}_1 a_w|\mathcal{E}_0|\sin(\zeta)\ . \tag{8c}$$

The equilibrium is characterized by $d_z|\mathcal{E}_0|=0$ and $\partial_z h=0$. This leads to

$$d_z\phi=\frac{\mu_0 e^2 c a_w \mathcal{K}_1}{|\mathcal{E}_0|}\int_1^{+\infty}\frac{dp}{2\sqrt{p}}\frac{1}{2\pi}\times\int_0^{2\pi}d\zeta\, h_0(\zeta,p)\exp(-i\zeta)$$

$$=\nu_r=\text{const}\ , \tag{9}$$

$$h_0(\zeta,p)=f(H_0(\zeta,p))\ , \tag{10}$$

where f is any function and H_0 is the periodic Hamiltonian determined by Eqs. (8b) and (8c) with $d_z\phi=\nu_r$ (the calculation of ν_r is detailed in Appendix A):

$$H_0(\zeta,p)=(k_w-\nu_r)p-\tfrac{1}{2}k_L(1+a_w^2/2)\ln(p)+\tfrac{1}{2}\mathcal{K}_1 a_w|\mathcal{E}_0|\cos(\zeta)\ . \tag{11}$$

This Hamiltonian has elliptic fixed points given by

$$\zeta=\zeta_n=\pi+2\pi n\ ,\qquad p=p_r=\tfrac{1}{2}k_L(1+a_w^2/2)/(k_w-\nu_r)\ . \tag{12}$$

Let us concentrate first on deeply trapped electrons, that is, let us consider an equilibrium electronic distribution $h_0(\zeta,p)=f(H_0(\zeta,p))$, where f is peaked at the minimum value of the Hamiltonian, $H_0(\zeta=\pi,p=p_r)$ so that the electron motion is harmonic. In this case, one can then readily obtain the value ν_h of ν_r from Eqs. (9) and (4):

$$\nu_h=-\frac{\mu_0 e^2 a_w \mathcal{K}_1 \rho_e}{2\sqrt{p_r}|\mathcal{E}_0|m}\ . \tag{13}$$

Actually, this formula involves the resonant energy $\sqrt{p_r}$, which is itself a function of ν [Eq. (12)]. One has therefore to solve a quadratic equation to find the exact value of ν_r. Since ν_h will appear as a coupling constant for the sideband growth with deeply trapped electrons, it is useful to notice that a rough estimate gives $\nu_h=(\Omega_h^2/k_w)(E_{\text{elec}}/E_{\text{las}})$, where Ω_h is the pulsation of the harmonic motion of the electrons at the bottom of the wells. For a typical case where $E_{\text{elec}}\simeq E_{\text{las}}$ inside the optical cavity, we get that $\nu_h\simeq\Omega_h^2/k_w\ll\Omega_h$.

The equilibrium described by Eqs. (8)–(11) is unstable when a new laser mode is assumed to have a small but nonzero amplitude, which generates a non-2π-periodic perturbation. Now, the Vlasov equation (8a) and the Hamiltonian (11) have to be implemented by new terms proportional to the sideband modes $\mathcal{E}_n$ and $\mathcal{E}_{-n}$, where n labels the relative frequency shift n/N. The dynamical equations for the laser modes $\mathcal{E}_{\pm n}$ and the perturbed density $h=h_0+h_1$ can be linearized in $\mathcal{E}_{\pm n}$ and h_1 to calculate the first-order evolution of the sideband modes. The details of this calculation are given in Appendix B, and we obtain

$$(\beta_n+id_z)\mathcal{Y}_n=\tfrac{1}{2}\nu_h\Omega_h\left[1+\frac{n}{N}\right]\times\int_0^z dz'\sin[\Omega_h(z-z')]\times[\mathcal{Y}_n(z')-\mathcal{Y}^*_{-n}(z')]\ , \tag{14}$$

where $\mathcal{Y}_n(z)\equiv\mathcal{E}_n(z)\exp(i\beta_n z)$ and $\beta_n\equiv\nu_h+(n/N)(\nu_h-k_w)$.

It appears, as expected, that symmetrical sidebands are coupled, each pair being independent of the others as long as we remain in the perturbative domain, at the first

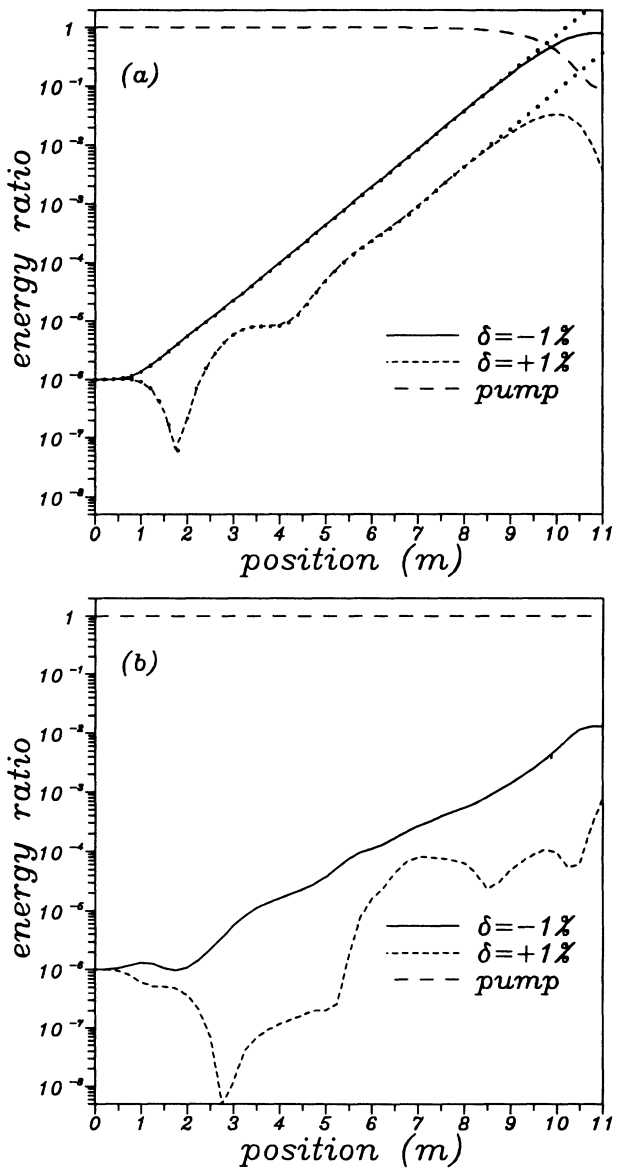

FIG. 3. Typical behavior of two coupled symmetrical sideband modes, with a relative frequency shift $\delta=n/N=\pm1\%$, for (a) electrons initially trapped at the bottom of the well, obtained with Eq. (5) (dotted lines) and with a full multifrequency numerical simulation of the Maxwell-Vlasov equations (2) and (3) (solid and broken lines). One can see the transient and exponential regimes, and finally the saturation regime where perturbation and Eq. (15) fail. Energies are in units of the pump-mode energy and position should be compared to the synchrotron length $L_s\simeq3.4$ m and the wiggler length $L_w=2m$ in this case; (b) a realistic nonbunched initial condition, obtained with a full multifrequency low-noise numerical simulation of the Maxwell-Vlasov equations. We recover qualitative features of the idealized case (asymmetrical instability with a depletion of the high-frequency sideband), except for a delay due to a preliminary bunching phase.

order. Note that the "natural" laser variable $\mathcal{Y}$ is the electric field with a phase shift $i\beta_n z$; this is consistent with the standard choice made, for instance, in [18]. However, we do not assume here that $\mathcal{Y}$ varies slowly either in amplitude or in phase. Furthermore, we do not assume any peculiar form for the sideband evolution, so that we can follow its whole history including the transient regime, from noise up to the exponential regime. The price we pay for having a description valid for high and nonexponential sideband gains is a restriction to the deeply trapped electrons. However, this will give us insight into the transient strong amplification of the sidebands, which is necessary if one wants to deal with realistic high-power FEL oscillators. Furthermore, this will enable us to validate the numerical simulations performed in more realistic situations. A natural way for extending the above treatment to a general initial equilibrium electronic distribution is presented in Sec. IV.

The evolution of the sidebands as given by Eq. (14) is nonlocal in time. However, taking advantage of the simple sine form of the kernel, one can reduce Eq. (14) to a simple matrix differential equation. Defining

$$A_n \equiv \mathcal{Y}_n + \mathcal{Y}^*_{-n}, \quad \Pi_n \equiv i(\mathcal{Y}_n - \mathcal{Y}^*_{-n}),$$
$$P_n \equiv i\int_0^z dz' \sin[\Omega_h(z-z')]\Pi_\delta(z'),$$
$$Q_n \equiv -i\int_0^z dz' \cos[\Omega_h(z-z')]\Pi_n(z'),$$

one obtains

$$id_z \begin{bmatrix} A \\ \Pi \\ P \\ Q \end{bmatrix} = \begin{bmatrix} \delta(k_w-\nu) & i\nu & -\nu & 0 \\ -i\nu & \frac{n}{N}(k_w-\nu) & -i\frac{n}{N}\nu\Omega & 0 \\ 0 & 0 & 0 & -i\Omega \\ 0 & 1 & i\Omega & 0 \end{bmatrix} \times \begin{bmatrix} A \\ \Pi \\ P \\ Q \end{bmatrix}. \tag{15}$$

This equation shows that the sideband instability for trapped electrons at the bottom of the well is essentially controlled by two parameters: the synchrotron frequency Ω_h (related to the amplitude $|\mathcal{E}_0|$ of the pump mode) and the phase derivative $\nu_h = d_z\phi$ (related to the phase velocity of the pump mode). The sideband growth rates for a given initial condition $\mathcal{E}_{\pm n}(z=0)$ are controlled by the eigenvalues of the matrix in Eq. (15). The eigenvalue of largest imaginary part gives the sideband growth rate in the exponential regime; since both coupled sidebands $\mathcal{E}_{\pm n}$ will in general (but not necessarily) have a component on the corresponding eigenvector, they will have the same exponential growth rate [Fig. 3(a)]. However, since they have a different history during the transient regime, their gains for one pass will in general be different. Furthermore, it must be realized that most often in realistic situations the asymptotic regime is not attained within the wiggler length. In particular, even though they have the same asymptotic exponential growth rate, the coupled modes may have very asymmetrical behaviors when a wiggler of finite length is considered [see $L_w = 2m$, for instance, in Fig. 3(a)], which is in general the case when dealing with oscillators: the transient regime lasts one or a few synchrotron lengths, and in an oscillator at saturation the synchrotron period of the electrons in the ponderomotive well is precisely of the order of magnitude of the wiggler length.

The study of the largest imaginary part eigenvalue of the matrix in Eq. (15) shows that there is, as expected, a resonance between the synchrotron motion of the electrons at the bottom of the potential wells and the beating between the pump and sideband modes, so that the exponential gain is peaked at $n/N = \Omega_h/k_w$ [Fig. 4(a)]. Equation (14) describes the time-dependent building of this resonance.

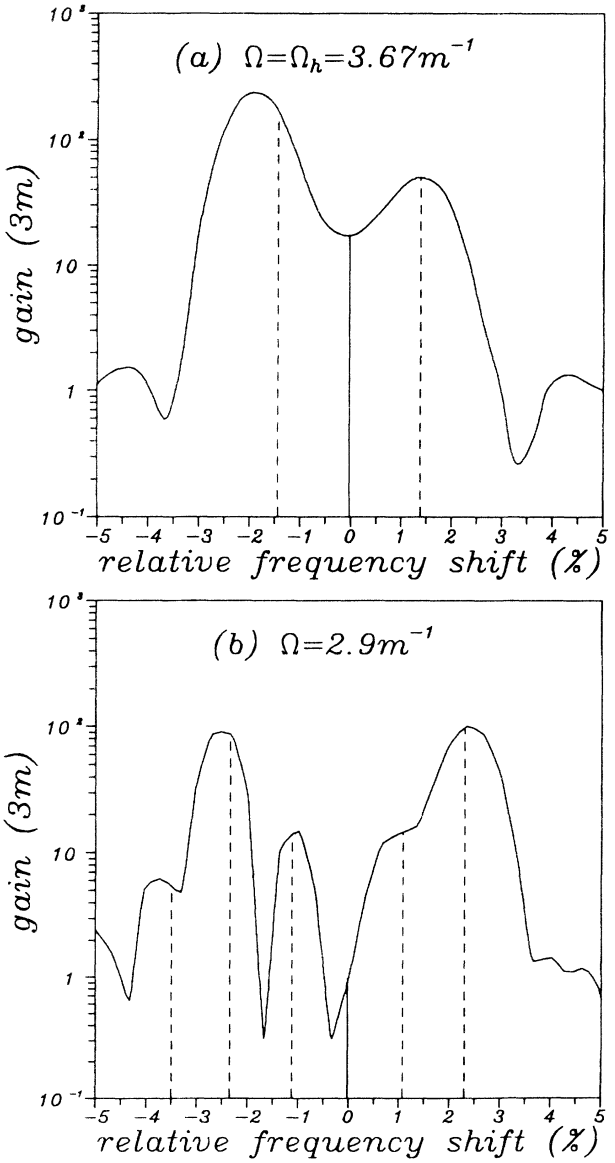

FIG. 4. One-pass gain curves for two equilibrium initial conditions labeled with their synchrotron frequency Ω. The positions of the resonant frequencies $n/N = j\Omega/k_w$ are also indicated. Since the transient regime is different for symmetrical sidebands, these curves are not symmetrical.

IV. SIDEBAND GROWTH FOR NONDEEPLY TRAPPED ELECTRONS

Let us now consider the case of a general initial equilibrium electronic distribution. Since we deal with the linear regime, we can consider the independent contributions of distributions concentrated on generic invariant curves of H_0. The integro-differential structure of Eq. (14) is preserved:

$$(\beta_n + id_z)\mathcal{Y}_n = \tfrac{1}{2}\nu_h \Omega_h \left[1+\frac{n}{N}\right] \times \int_0^z dz' \mathcal{K}(z-z')[\mathcal{Y}_n(z') - \mathcal{Y}^*_{-n}(z')] , \tag{16}$$

where the kernel $\mathcal{K}(z)$ is now an anharmonic $2\pi/\Omega$ periodic function, where Ω is the pulsation of the motion on the considered invariant curve. Using the action-angle variables, it is possible to give in closed form an expression for this kernel [18], but the evolution equation can no longer be easily put under a simple form similar to Eq. (15). However, expanding the kernel as a Fourier series and keeping only a finite number k of terms,

$$\mathcal{K}(z) = \sum_{j=1}^{k} \mathcal{K}_j \sin(j\Omega z) , \tag{17}$$

we can generalize (15) with a square matrix of dimension $(2+2k)$. This formulation shows that the beating wave due to the sideband will resonate with all the present harmonics $\mathcal{H}_j$ of the electronic motion, at $n/N = j\Omega/k_w$. As Ω goes to zero close to the separatrix, one observes more and more resonances. This remark is used in [18] where it is shown that in the low-gain asymptotic regime the sideband generation is mainly due to electrons close to the separatrix.

We performed very-low-noise numerical simulations to picture the sideband evolution including the transient regime, starting with an equilibrium electronic distribution concentrated on an invariant curve of H_0. With an initial ratio between the sideband and pump mode energies of 10^{-6}, an optimization of the electron sampling allows us to inhibit numerical noise down to 10^{-10}. We found features that remain very similar to the situation described in Sec. III: although they have equal asymptotic exponential growth rates, the high- and low-frequency symmetrical sidebands have very different histories, including a strong depletion of the high-frequency sideband for short times. This is why the finite-length sideband gain curves (Fig. 4) are not symmetrical and may have a complicated shape. Nevertheless, the resonances at $n/N = j\Omega/k_w$ are visible for frequency shifts such that the asymptotic regime has been attained.

It appears in Fig. 4 that the envelope of the resonances occurring for different orbits, either deep in the well or not, remains roughly constant. This illustrates the prediction of [18] where it is stated that the same sideband frequency is generated either by deeply trapped electrons or by the summation of the resonances for electrons close to the separatrix.

However, in an actual standard experiment the initial electron distribution is uniform in ψ. For an oscillator, it is necessary to bridge the gap between academic approaches and the more realistic results presented in Sec. II. For that purpose, we performed very low-noise one-pass numerical simulations starting from a nonbunched electron distribution.

Some results for nonbunched beams are depicted in Fig. 3(b). Qualitatively, they look very much like the academic case of Fig. 3(a). One difference, however, is the appearance of a preliminary phase (about 1.5 m in our case) during which the electrons bunch, and the electron plus laser system reaches a quasiequilibrium state similar to the initial state of Sec. III; this is supported by noticing that it takes about the same bunching time (1.5 m) to the phase derivative ν of the laser field for reaching its "asymptotic" value. Only in a second phase does the electron motion begin to feed the sidebands in a way similar to the idealized case, beginning with a strong depletion of the high-frequency sideband. Of course, except if the coupling is too weak, sidebands will begin to grow even during the bunching phase. Now in a standard experiment where the fundamental mode has been brought to saturation, the synchrotron and wiggler lengths are of the same order of magnitude. Therefore electrons have just enough time to bunch, so that they do not actually experience the second phase, and *a fortiori* they never see the exponential regime. This shows a major limitation of the usual academic sideband analysis for FEL oscillators.

V. SIDEBAND INSTABILITY AND TAPERING IN AN AMPLIFIER FEL

To investigate the effect of tapering, we first consider one-pass simulations in a long wiggler. The initial value of a_w is supposed to be large enough to support a strong tapering without eliminating the coupling at the end of the wiggler. This is typically the situation of Ref. [4] where it appears that sidebands are strongly inhibited.

We consider the FEL parameters given in [4]: a 25-m-long wiggler is tapered from $a_w = 1.7$ down to $a_w = 0.4$. This implies that the resonant electron energy is decreased by an amount of 35%. In accordance with [4], we observe a strong depletion of the sideband due to the tapered wiggler. This shows that 1D simulations are relevant to investigate sideband generation despite the lack of gain focusing. This self-consistent 2D effect is responsible for some power enhancement [4], but is weakly coupled to sideband dynamics.

In Fig. 5, we plot the growth of two symmetrical typical sideband lines for uniform [Fig. 5(a)] and tapered [Fig. 5(b)] wigglers. For positions z larger than 5 m, the exponential growth rate decreases from 0.36 m^{-1} down to 0.16 m^{-1} from the uniform to the tapered case. According to [4], this leads at the end of the wiggler to a fundamental mode many decades above the rest of the spectrum. To clarify this, we compare three different approaches.

Approach 1. We perform a realistic simulation with a nonbunched initial condition (stars in Fig. 5). From this simulation, we measure the average trapping ratio over the wiggler length. We find 75% (45%) for the uniform

(tapered) wiggler.

Approach 2. We generalize the model developed in Sec. III by using an adiabatic assumption: Eq. (15) is unchanged, but now the synchrotron frequency Ω and the phase drift ν are functions of z. These functions depend on $a_w(z)$ and on the laser energy which is evaluated as the complementary variation of the resonant electron energy. We use this adiabatic generalization with the effective trapped charge (full lines in Fig. 5).

Approach 3. To check this adiabatic assumption, we also provide full numerical simulations for the dynamics of deeply trapped electrons (squares in Fig. 5). For uniform wigglers this fits perfectly Eq. (15) up to saturation [Fig. 3(a)]. For tapered wigglers, some differences can emerge because of inertial forces. Indeed [1], the ponderomotive potential $\sin(\psi)$ is incremented by a linear term $\psi d_z p_r$, where p_r depends on $a_w(z)$ [Eq. (12)]. The induced constant force will clearly shift the value of the phase derivative ν_h [Eq. (13)] used in Eq. (15) by an amount proportional to $d_z^2 p_r$.

For large values of z, the agreement between the three simulations shown in Fig. 5 is good. It can even be improved if one considers the instantaneous trapping ratio to solve Eq. (15). This corroborates clearly, for wigglers long compared to the synchrotron length, that the sideband instability is only due to trapped electrons [3]. More surprisingly, the collapse of the sideband gain is mainly due to the variation of instantaneous FEL parameters such as $a_w(z)$ or the trapping ratio and not to some inertial force induced by the time-dependent Hamiltonian. This is clearly shown by Fig. 6 where approaches 2 and 3 are compared for three different taperings.

This shows that, although the detrapping is the sign of nonadiabatic dynamics, the particles remaining in the bucket essentially follow an adiabatic dynamics. The usual picture based upon the nonadiabatic distortion of electronic motion in the bucket is clearly wrong in that case.

For small values of z in the tapered wiggler, Fig. 5(b) exhibits large discrepancies between the three computa-

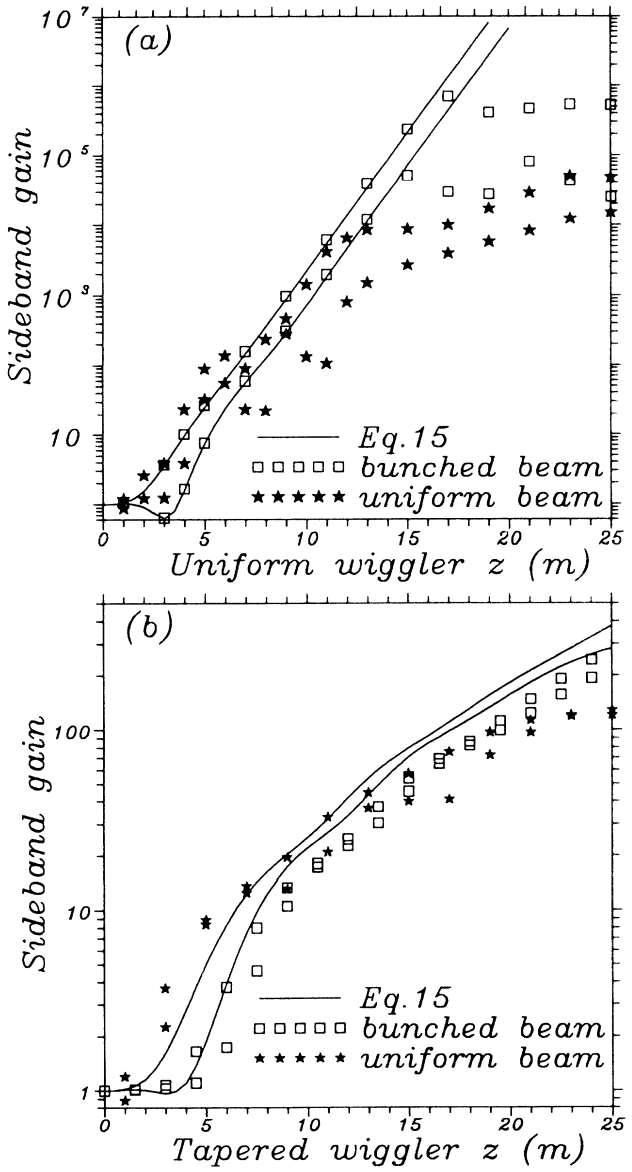

FIG. 5. Sideband gain curves for tapered and nontapered amplifiers. For each simulation, lower and upper sideband modes are presented. The stars are given by a realistic simulation assuming a uniform initial electron beam. The same simulation, but with a bunched beam (deeply trapped particles), provides the square points. The full line is obtained by solving within an adiabatic assumption the perturbation theory in Sec. III [Eq. (15)]. If the sideband is clearly depleted from the nontapered to the tapered wiggler, it is still large for short distances.

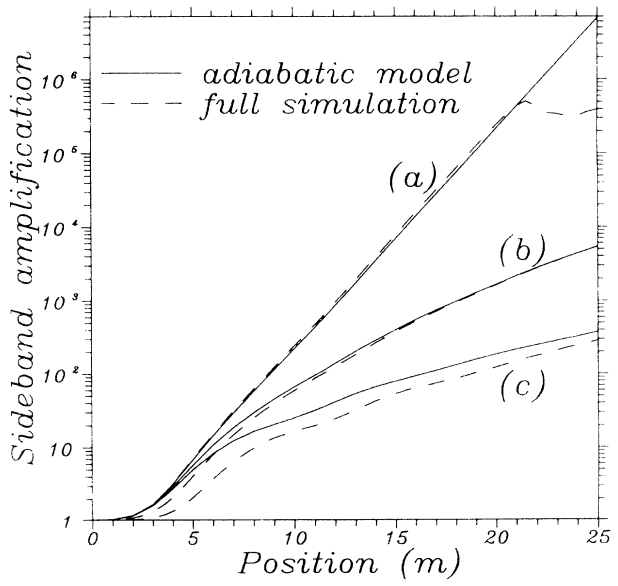

FIG. 6. Comparison for deeply trapped particles between the adiabatic model and full simulation (Sec. V). The agreement is correct for the uniform wiggler (curves *a*) and for a tapered wiggler where the wiggler parameter goes from $a_w=1.72$ down to $a_w=1.02$ (curves *b*). For a stronger tapering ($a_w=0.32$ at the end of the wiggler), we observe a slight difference (curves *c*). This shows that the effect of tapering on sideband generation is mainly explained by parameter variations and not by inertial forces.

tions. For trapped electrons, the realistic sideband evolution is delayed from the one given by Eq. (15). For nonbunched electrons, the growth rate is even larger. Such a large disagreement is not well understood and it illustrates the complexity of transient regimes where bunching mechanisms can induce delays.

Moreover, one observes that even with such a strong tapering rate, the effective sideband gain is still close to 10 after 5 m of tapered wiggler. Clearly, in an oscillator experiment, this would lead to a strong broadening. This is basically due to the fact that it is not possible to taper strongly the beginning of the wiggler since some bunching length is required before lowering the bucket. It is the case for simulations of Ref. [4] and Fig. 5 where the first two meters of the wiggler are not tapered.

To enforce this conclusion, we use a comparable strong parabolic tapering ($a_w = 1.7$ down to $a_w = 0.4$) in an oscillator computation with a 1-m-long wiggler. The trapping ratio goes from 75% down to 10% at $z = 0.5$ m because of the parabolic profile of the magnetic field. But, at the same time, the synchrotron length shortened at $L_w = 0.5$ m due to a strong efficiency enhancement. So, a large amount of trapped particles undergo a full synchrotron period which generates sidebands: after a large number of round-trips, we observed a broad-spectrum regime.

As an essential difference with oscillator experiments, it is not possible in an amplifier to speak about the asymptotic equilibrium. Indeed, it would imply that we push the dynamics for arbitrary large wiggler lengths, which is clearly impossible with a decreasing magnetic field. So, a tapered amplifier experiment is basically a finite-time experiment, such that sidebands can appear to be definitively suppressed. On the contrary, in an FEL oscillator, a realistic asymptotic regime is defined with an arbitrary number of round-trips. This basic distinction is emphasized by the following analysis.

VI. SIDEBAND INSTABILITY AND TAPERING IN AN FEL OSCILLATOR

We are now in a position to come back to the study of sideband generation in a tapered FEL oscillator, as it appears in Sec. II. Sideband computations in Sec. IV assume some given laser initial conditions (here both symmetrical sidebands of zero phase and equal amplitude). Since the symmetrical modes are coupled, the actual gain per pass, which relates the value $\mathcal{E}_{\pm n}(L_w)$ of the sidebands at the end of the wiggler to their value $\mathcal{E}_{\pm n}(0)$ at the entrance, is a 4×4 real matrix $\mathcal{G}$. This matrix can be obtained numerically by computing the laser field $\mathcal{E}_{\pm n}(L_w)$ with four different choices of the initial conditions $\mathcal{E}_{\pm n}(0)$. However, a scalar sideband gain can be defined as the maximum amplitude of the eigenvalues of $\mathcal{G}$. Comparing this gain to the cavity losses tells us whether or not the sideband instability will be triggered. This is what we did for tapered systems, for the parameters corresponding to Fig. 2. Although these sideband gain curves have a rather complicated shape, which is numerically difficult to stabilize, the thresholds are not very sensitive, and one can draw some semiquantitative conclusions. As expected, it appears that tapering lowers the sideband gain (Fig. 7) so that, in certain cases, it will drop below the losses: this is sideband inhibition. More generally, these gain curves provide a simple way to find the size of a filter necessary to eliminate the sideband for a given value of the cavity losses, provided the pump-mode amplitude and position are kept fixed (the following shows that the situation is actually more complicated).

The inspection of gain curves similar to those of Fig. 7 leads to the definition of region I in the map of Fig. 2: it is the regime where the sideband should not grow, according to the previous analysis. It appears that we are far from the end of the story, since we observe both low brightness spectra in region I and high brightness spectra outside region I (where the sideband instability is expected). Actually, it should not be forgotten that (i) the pump mode still evolves while the sideband develops and (ii) the system still has a history after the sideband instability, until saturation. Let us briefly review these two issues.

First, to analyze the sideband growth, we fixed the position and amplitude of the fundamental mode. But, in a realistic FEL oscillator, this amplitude varies continuously from noise up to saturation, and the corresponding sideband gain curve evolves accordingly. Therefore it is clearly not true that the sideband only develops after the fundamental mode has reached its saturation level. It happens that the sideband growth rate can be higher for a lower energy of the pump mode, so that sidebands can be observed for filters narrower than those predicted by only considering the saturation level of the pump mode. This is what happens in Fig. 2 for uniform wigglers ($\Delta B/B = 0$) and narrow filters ($\mathcal{F} < 3\%$).

Second, a careful analysis of the data in region II

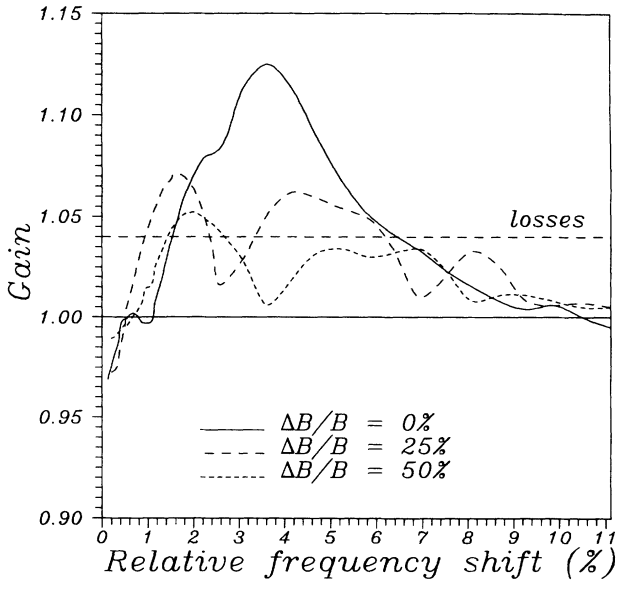

FIG. 7. Sideband gain curves for various values of the tapering amplitude $\Delta B/B$. Although tapering tends to lower the sideband gain, the inhibition can be made complete only with the help of a filter. The maximum authorized width for this filter may be determined from the comparison between the gain curve and the losses threshold.

shows that a final monochromatic laser field can result from a complicated dynamics due to mode competition. Various scenarios may occur depending on the filter width $\mathcal{F}$. With a very narrow filter ($\ll 1\%$), the linear gain is almost constant over the filter range, so that the spectrum at the beginning of the nonlinear regime is still flat, which is completely different from the usual situation where a monochromatic field is assumed. The evolution of this flat spectrum is not driven by the sideband instability but by mode competition [22], which leads to a monochromatic field with a frequency equal to the lower bound of the filter. This evolution can be interpreted as a boundary effect: each mode within the filter bandwidth is coupled by mode competition to its closest neighbors with higher and lower frequencies, except at the edge of the filter where the competition is roughly twice smaller. For an intermediate filter bandwidth, the scenario is different: a monochromatic laser field develops as usual, followed by a sideband which reaches the same order of magnitude. But then the filter prevents the generation of a third frequency, and mode competition between the pump and sideband modes leads to the elimination of the pump mode, and to the observed high brightness. Such a nontrivial effect of filtering illustrates the interaction between different modes in the nonlinear regime.

VII. CONCLUSION

The optimization of efficiency and monochromaticity in high-power FEL's makes necessary an improved understanding of the mechanisms controlling spectral broadening effects in uniform as well as in tapered wigglers. We presented first an investigation based on full numerical simulations for tapered FEL oscillators. This shows that tapering does not always provide an efficient way to control the spectral evolution: it can be overwhelmed by broadening mechanisms which induce a complex electronic phase-space structure. Nevertheless, by coupling a filter and a tapered wiggler, we can exhibit the connection between tapering and spectral dynamics; this generates the intricate map given in Fig. 2, resulting from the antagonisms between tapering and the broadening mechanisms.

In order to understand, and eventually to control, the transition between narrow- and broad-spectrum regimes, it is necessary to go beyond the numerical investigations presented in Fig. 2. Since the sideband instability is given as the driving mechanism responsible for spectral broadening, we devoted an important part of this paper to its analysis.

Long-amplifier investigations in Sec. V emphasize (i) the important role of the detrapping in the sideband inhibition and (ii) the adiabaticity of the trapped particles motion even for strong tapering. In practice, the decrease of the exponential growth rate can lead, for long but finite wigglers, to a strong depletion of the sideband. But, in general, this decrease is not large enough to prevent sideband generation in an FEL oscillator. From a basic point of view, this stresses that the sideband cannot be said to be fully destroyed in tapered amplifiers.

For FEL oscillators, the standard presentation of the sideband instability, starting from an equilibrium with deeply trapped electrons and assuming an exponential growth rate, is largely irrelevant for the prediction of the spectral behavior at saturation. There are two kinds of reasons for this.

(i) First, such an analysis of the sideband instability overlooks very important issues. At saturation for the fundamental laser mode, the synchrotron and wiggler lengths are roughly equal. Even in strongly tapered wigglers with shortened synchrotron length L_S, trapped electrons run over a period L_S and can generate sidebands.

As detailed in Sec. III, this implies that the sideband gain per pass is given by the transient regime, which is very different from the exponential gain. Furthermore, it is known that electrons that are not deeply trapped give an important contribution to the exponential sideband gain, especially those near the separatrix. Numerical simulations show (Fig. 4) that this is true even in the transient regime. The approach developed in Sec. III could be extended to take into account more and more anharmonic orbits; however, it will not enable us to consider orbits very close to the separatrix. Therefore, further developments are required to make the connection between the attractive idea of resonance resummation close to the separatrix [18], and the approaches available for the transient regime. But, even if this was done, it should be taken into account that the initial condition for the electrons is not an equilibrium, but a monochromatic translationally invariant beam. Even a full understanding of the sideband instability starting with an equilibrium as an initial condition would not make available any quantitative prediction for the realistic sideband evolution: the sideband evolutions with nonbunched and equilibrium initial conditions present the same general outlook only after a bunching phase (Fig. 3).

(ii) Second, the sideband instability is far from being the only mechanism involved in the long-term spectral evolution. For example, the FEL oscillator behavior is also driven by mode competition or difference frequency generation, as presented in paper I. Examining in detail the spectral behavior versus filter and tapering (Fig. 2), we were led to divide the plane into different regions dominated by different mechanisms. For very narrow filters (region I), the sideband instability is inhibited by the combined effect of filtering and cavity losses (Fig. 7), so that we get a monochromatic laser field with very high brightness ($\mathcal{B} \gg 3$). On the contrary, very wide filters (region IV) allow a broad spectrum with universal brightness ($\mathcal{B} \leq 1$), extensively studied in paper I, and which is driven by a sequence of sideband instabilities and difference-frequency generations. But for filters of intermediate width, and depending on tapering rates, we observe complex equilibria. For example, one can observe a transition region (region III) where the spectrum is broad, but narrower than the filter ($1 \leq \mathcal{B} \leq 3$). Finally, in region II the asymptotic spectrum is very narrow (although the sideband does develop), due to nonlinear mode competition within a small available frequency interval.

This paper has shown the multiplicity of the possible

spectral evolutions allowed by the FEL dynamics with strong couplings. A perturbative analysis working in the small-field limit is unable to explain these global results presented in Fig. 2. As suggested in paper I, it is therefore necessary to develop approaches complementary to the sideband instability or the difference frequency generation to understand the spectral evolution and the asymptotic equilibrium as a whole.

ACKNOWLEDGMENT

The Laboratoire de Spectroscopie Hertzienne is "Unité de Recherche Associée du Centre National de la Recherche Scientifique No. 249."

APPENDIX A: CALCULATION OF THE PHASE DRIFT ν_r AT EQUILIBRIUM

We consider an equilibrium electronic distribution $h_0(\zeta,p)=f(H_0(\zeta,p))$. The normalization [Eq. (4)] and the phase drift [Eq. (9)] give

$$\rho_e = mc\frac{1}{2\pi}\int_0^{2\pi} d\zeta \int_1^{+\infty} dp\, h_0(\zeta,p) ,$$

$$\nu_r = A\int_1^{+\infty} dp \frac{1}{2\pi}\int_0^{2\pi} d\zeta\, h_0(\zeta,p)\exp(-i\zeta) ,$$

with $A=\mu_0 e^2 c a_w \mathcal{H}_1/2\sqrt{p_r}|\mathcal{E}_0|$. Since $(p-p_r)/p_r$ remains small, we only kept the lowest order in $(p-p_r)/p_r$. The Hamiltonian is

$$H_0(\zeta,p)=B(1-p/p_r)^2+C\cos\zeta ,$$

where $B=\frac{1}{2}k_L(1+\frac{1}{2}a_w^2)$ and $C=\frac{1}{2}\mathcal{H}_1 a_w|\mathcal{E}_0|$, and the distribution h_0 can be decomposed in elementary equilibrium distributions each characterized by an energy $\mathcal{W}=(2\mu-1)/C$ (we will consider trapped electrons: from the bottom to the top of the potential well, $\mathcal{W}$ ranges from $-C$ to C, and μ ranges from 0 to 1):

$$h_0(\zeta,p)=f(H_0(\zeta,p))=\int d\mathcal{W} f(\mathcal{W})\delta(H_0(\zeta,p)-\mathcal{W}) .$$

This leads to

$$\rho_e = mc\int d\mathcal{W} f(\mathcal{W})\frac{1}{2\pi}\int_0^{2\pi} d\zeta \int_1^{+\infty} dp\, \delta(H_0(\zeta,p)-\mathcal{W}) ,$$

$$\nu_r = A\int d\mathcal{W} f(\mathcal{W})\frac{1}{2\pi}\int_{b0}^{2\pi} d\zeta \exp(-i\zeta) \times \int_1^{+\infty} dp\, \delta(H_0(\zeta,p)-\mathcal{W}) .$$

The p integral is readily evaluated: it is zero for $\mathcal{W}/C-\cos\zeta<0$, and

$$\int_1^{+\infty} dp\, \delta(H_0(\zeta,p)-\mathcal{W}) = \frac{1}{2\sqrt{BC}}(\mathcal{W}/C-\cos\zeta)^{-1/2} \quad \text{for } \mathcal{W}/C-\cos\zeta>0 ,$$

so that

$$\rho_e = \frac{mc}{2\sqrt{BC}}\int d\mathcal{W} f(\mathcal{W})\frac{1}{\pi}\int_0^{\phi} d\zeta (\mathcal{W}/C+\cos\zeta)^{-1/2} ,$$

$$\nu_r = \frac{-A}{2\sqrt{BC}}\int d\mathcal{W} f(\mathcal{W})\frac{1}{\pi} \times \int_0^{\phi} d\zeta \cos\zeta(\mathcal{W}/C+\cos\zeta)^{-1/2} ,$$

where $\mathcal{W}/C-\cos\zeta>0$ for $\zeta\in[\pi-\phi,\pi+\phi]$. With $u=\mu^{-1/2}\sin(\zeta/2)$, the ζ integrals are complete elliptic integrals of the first and second kind [23]:

$$\int_0^{\phi} d\zeta(\mathcal{W}/C+\cos\zeta)^{-1/2} = \int_0^1 du\,(1-\mu u^2)^{-1/2}(1-u^2)^{-1/2} = K(\mu) ,$$

$$\int_0^{\phi} d\zeta\cos\zeta(\mathcal{W}/C+\cos\zeta)^{-1/2} = \int_0^1 du\,(1-\mu u^2)^{-1/2}(1-2\mu u^2)(1-u^2)^{-1/2} = 2E(\mu)-K(\mu) ,$$

so that

$$\rho_e = \frac{mc}{2\pi\sqrt{BC}}\int d\mathcal{W} f(\mathcal{W})K(\mu) ,$$

$$\nu_r = \frac{-A}{2\pi\sqrt{BC}}\int d\mathcal{W} f(\mathcal{W})\{2E(\mu)-K(\mu)\} .$$

The normalization of the distribution f can be eliminated from these equations, so that

$$\nu_r = \nu_h\frac{\int d\mathcal{W} f(\mathcal{W})\{2E(\mu)-K(\mu)\}}{\int d\mathcal{W} f(\mathcal{W})K(\mu)} ,$$

where ν_h is given by Eq. (13). If f is a Dirac distribution centered on a given energy $\mathcal{W}$, this reduces to

$$\nu_r = \nu_h \mathcal{F}\left[\frac{1+\mathcal{W}/C}{2}\right] \quad \text{with } \mathcal{F}(\mu)=2\frac{E(\mu)}{K(\mu)}-1 .$$

At the bottom of the well $\mathcal{W}=-C$ and $\mu=0$, so that we find $\nu_r=\nu_h$. Although the integrals present logarithmic singularities at the separatrix ($\mathcal{W}=C$ and $\mu=1$), the function $\mathcal{F}$ is regular and ranges from 1 to -1 when the equilibrium trajectory ranges from the bottom to the top of the potential well.

APPENDIX B: DERIVATION OF THE FIRST-ORDER EQUATIONS FOR THE SIDEBAND GROWTH

Once an equilibrium distribution is given, we have seen that the natural phase variable for the electrons is $\zeta=\psi-\nu_r z$ where ν_r has been calculated in Appendix A. The dynamical equations [Eqs. (2) and (3)] can be restated with this variable, which induces a corresponding change of variable for the electric field phases:

$$\mathcal{Y}_n = \mathcal{E}_n \exp i\beta_n z \quad \text{with } \beta_n=\nu_r+\frac{n}{N}(\nu_r-k_w) .$$

One finds

$$(\beta_n + id_z)\mathcal{Y}_n = \mu_0 e^2 c a_w \mathcal{H}_1 \times \int_1^{+\infty} \frac{dp}{2\sqrt{p}} \frac{1}{2\pi N} \int_0^{2\pi N} d\zeta\, h(z,\zeta,p) \times \exp\left[-i\left[1+\frac{n}{N}\right]\zeta\right] ,$$

$$[\partial_z + (\partial_p H)\partial_\zeta - (\partial_\zeta H)\partial_p] h(z,\zeta,p) = 0 ,$$

$$\partial_p H = (k_w - \nu_r) - k_L(1 + a_w^2/2)/2p ,$$

$$-\partial_\zeta H = \tfrac{1}{2}\mathcal{H}_1 a_w \mathrm{Im} \sum_{n\,(\ll N)} \mathcal{Y}_n \exp\left[i\left[1+\frac{n}{N}\right]\zeta\right] .$$

The electronic density and the Vlasov operator can be decomposed into an equilibrium part and a perturbation, $h = h_0 + h_1$ and $D = D_0 + D_1$ with

$$D_0 = [\partial_z + (\partial_p H_0)\partial_\zeta - (\partial_\zeta H_0)\partial_p] ,$$

$$D_1 = \tfrac{1}{2}\mathcal{H}_1 a_w \mathrm{Im} \sum_{n\,(\neq 0)} \mathcal{Y}_n \exp\left[i\left[1+\frac{n}{N}\right]\zeta\right]\partial_p ,$$

so that, to the first order in $\mathcal{Y}_{n\neq 0}$ and h_1, the dynamical equations become

$$(\beta_n + id_z)\mathcal{Y}_n = \mu_0 e^2 c a_w \mathcal{H}_1 \times \int_1^{+\infty} \frac{dp}{s\sqrt{p}} \frac{1}{2\pi N} \int_0^{2\pi N} d\zeta\, h_1(z,\zeta,p) \times \exp\left[-i\left[1+\frac{n}{N}\right]\zeta\right] ,$$

$$D_0 h_1 = -D_1 h_0 .$$

Now we deal with deeply trapped electrons, so that h_0 and h_1 are concentrated around the resonant points $(\zeta = (2m+1)\pi, p = p_r)$:

$$h_0(\zeta,p) = \sum_m h_0^0(\zeta - (2m+1)\pi, p - p_r) ,$$

$$h_1(z,\zeta,p) = \sum_m h_1^m(z,\zeta - (2m+1)\pi, p - p_r) ,$$

where the functions h_0^0 and h_1^m are peaked around the origin (the functions h_1^m are different from one another, so that the perturbation h_1 is not 2π periodic). We can now expand D_0 around each resonant point:

$$D_0 = \{\partial_z + A(p - p_r)\partial_\zeta - B[\zeta - (2m+1)\pi]\partial_p\} ,$$

with

$$A = \frac{2(k_w - \nu_h)^2}{k_L(1 + \frac{1}{2}a_w^2)} , \quad B = \tfrac{1}{2}\mathcal{H}_1 a_w \mathcal{Y}_0 , \quad \Omega_h = (AB)^{1/2} .$$

It is then useful to use variables proportional to the action and angle centered on each resonant point:

$$\zeta = (2m+1)\pi - A^{1/2} J_m \cos\theta_m , \quad p = p_r + B^{1/2} J_m \sin\theta_m ,$$

so that in the vicinity of $(\zeta = (2m+1)\pi, p = p_r)$,

$$h_0(\zeta,p) = h_0^0(J_m) , \quad h_1(z,\zeta,p) = h_1^m(z,J_m,\Theta_m) ,$$

$$D_0 = (\partial_z + \Omega_h \partial_{\theta m}) ,$$

$$D_1 = -B^{1/2} \mathrm{Im} \sum_{n\,(\neq 0)} (\mathcal{Y}_n/\mathcal{Y}_0) \exp\left[i\frac{n}{N}(2m+1)\pi\right] \times \left[\sin(\theta_m)\frac{d}{dJ_m} + \frac{1}{J_m}\cos(\theta_m)\frac{d}{d\theta_m}\right] .$$

The first-order Vlasov equation can now be written around each resonant point:

$$(\partial_z + \Omega_h \partial_\theta) h_1^m(z,J,\theta) = B^{1/2} \sin(\theta) \frac{dh_0^0}{dJ} \times \mathrm{Im} \sum_{n\,(\neq 0)} [\mathcal{Y}_n(z)/\mathcal{Y}_0] \exp\left[i\frac{n}{N}(2m+1)\pi\right] .$$

This equation is readily integrated by changing the variable θ into $\theta - \Omega_h z$:

$$h_1^m(z,J,\theta) = B^{1/2} \frac{dh_0^0}{dJ} \int_0^z dz' \sin[\theta - \Omega_h(z - z')] \mathrm{Im} \sum_{n\,(\neq 0)} [\mathcal{Y}_n(z')/\mathcal{Y}_0] \exp\left[i\frac{n}{N}(2m+1)\pi\right] .$$

We can now go to the equation on the electromagnetic field:

$$(\beta_n + id_z)\mathcal{Y}_n = D \int_1^{+\infty} dp \frac{1}{2\pi N} \int_0^{2\pi N} d\zeta \sum_m h_1^m(z,\zeta - (2m+1)\pi, p - p_r) \exp\left[-i\left[1+\frac{n}{N}\right]\zeta\right] ,$$

with $D = \mu_0 e^2 c a_w \mathcal{H}_1 / 2\sqrt{p}$. Since each of the h_1^m is peaked in a given 2π interval in ζ, this can be rewritten,

$$(\beta_n + id_z)\mathcal{Y}_n = D \int_1^{+\infty} dp \frac{1}{2\pi N} \int_0^{2\pi} d\zeta \sum_m h_1^m(z,\zeta - \pi, p - p_r) \exp\left[-i\left[1+\frac{n}{N}\right](\zeta + 2m\pi)\right] .$$

Since h_1^m is peaked at $\zeta = \pi$, we can expand the exponential to the first order in $\zeta = \pi$ ($\zeta = \pi$ gives a zero contribution):

$$(\beta_n + id_z)\mathcal{Y}_n = i\left[1+\frac{n}{N}\right] D\frac{1}{2\pi N}\sum_m \int_1^{+\infty} dp \int_0^{2\pi} d\zeta(\zeta-\pi) h_1^m(z,\zeta-\pi,p-p_r)\exp\left[-i\frac{n}{N}(2m+1)\pi\right] .$$

Going to the (J,θ) variables (the Jacobian is $\Omega_h J$), this becomes

$$(\beta_n + id_z)\mathcal{Y}_n = -iA^{1/2}D\left[1+\frac{n}{N}\right]\frac{1}{2\pi N}\sum_m \int \Omega_h J^2 dJ\, d\theta \cos(\theta) h_1^m(z,J,\theta)\exp\left[-i\frac{n}{N}(2m+1)\pi\right] .$$

Let us put the expression of h_1^m in this formula; the θ integral is trivial since we are at the bottom of the well where the motion is harmonic. The J integral can be performed by parts, which leads to the density ρ_e:

$$(\beta_n + id_z)\mathcal{Y}_n = iD\left[1+\frac{n}{N}\right]\frac{\Omega_h \rho_e}{mc\mathcal{Y}_0}\int_0^z dz' \sin[\Omega_h(z'-z)] \times \frac{1}{N}\sum_{\substack{m,k \\ k\neq 0}} \mathrm{Im}\left[\mathcal{Y}_k \exp\left[i\frac{k}{N}(2m+1)\pi\right]\right]\exp\left[-i\frac{n}{N}(2m+1)\pi\right] .$$

The summation on m (position of the resonant points along the electron beam) and on k (laser mode coupled to $\mathcal{Y}_n$) leads to

$$(\beta_n + id_z)\mathcal{Y}_n = iD\left[1+\frac{n}{N}\right]\frac{\Omega_h \rho_e}{mc\mathcal{Y}_0}\int_0^z dz' \sin[\Omega_h(z'-z)](-i/2)[\mathcal{Y}_n(z') - \mathcal{Y}^*_{-n}(z')] ,$$

where the asterisk denotes the complex conjugate. This can be rewritten

$$(\beta_n + id_z)\mathcal{Y}_n = \frac{1}{2}\nu_h \Omega_h \left[1+\frac{n}{N}\right]\int_0^z dz' \sin[\Omega_h(z-z')][\mathcal{Y}_n(z') - \mathcal{Y}^*_{-n}(z')] .$$

[1] N. M. Kroll, P. L. Morton, and M. N. Rosenbluth, IEEE J. Quantum Electron. **QE-17**, 1436 (1981).

[2] R. A. Freedman and W. B. Colson, Opt. Commun. **52**, 409 (1985).

[3] W. B. Colson, in *Free-Electron Generators of Coherent Radiation,* edited by C. A. Brau, SPIE Proc. Vol. 453 (SPIE, Bellingham, WA, 1984), p. 290.

[4] B. Hafizi, A. Ting, P. Sprangle, and L. M. Tang, Phys. Rev. A **38**, 197 (1988); Phys. Rev. Lett. **64**, 180 (1990).

[5] N. M. Kroll and M. N. Rosenbluth, *Physics of Quantum Electronics,* edited by S. F. Jacobs *et al.* (Addison-Wesley, Reading, MA, 1980), Vol. 7, p. 147; S. Riyopoulos and C. M. Tang, Phys. Fluids **31**, 3387 (1988).

[6] D. C. Quimby, in *Free-Electron Lasers,* edited by B. E. Newman, SPIE Proc. Vol. 738 (SPIE, Bellingham, WA, 1978), p. 103.

[7] R. W. Warren *et al.*, Nucl. Instrum. Methods Phys. Res. Sect. A **285**, 1 (1989).

[8] J. C. Goldstein, in *Free-Electron Generators of Coherent Radiation,* (Ref. [3]), p. 2.

[9] J. C. Goldstein, B. E. Newnam, and R. W. Warren, Nucl. Instrum. Methods Phys. Res. Sect. A **272**, 150 (1988).

[10] D. C. Quimby, J. M. Slater, and J. P. Wilcoxon, IEEE J. Quantum Electron. **QE-21**, 979 (1985).

[11] D. W. Feldman *et al.*, Nucl. Instrum. Methods Phys. Res. Sect. A **285**, 11 (1989).

[12] J. L. Ferrer and D. Iracane, Nucl. Instrum. Methods Phys. Res. Sect. A **318**, 564 (1992).

[13] W. M. Sharp and S. S. Yu, Phys. Fluids B **2**, 581 (1990).

[14] J. N. Elgin, Nucl. Instrum. Methods Phys. Res. Sect. A **285**, 144 (1989).

[15] N. M. Rosenbluth, W. V. Wong, and B. N. Moore, Phys. Fluids B **2**, 1635 (1990).

[16] T. Y. B. Yang and R. C. Davidson, Phys. Fluids B **2**, 2456 (1990).

[17] S. Riyopoulos, Phys. Fluids B **3**, 2684 (1991).

[18] J. N. Elgin, Phys. Rev. A **43**, 2514 (1991).

[19] W. B. Colson and S. K. Ride, Phys. Lett. **76A**, 379 (1980).

[20] W. B. Colson and R. A. Freedman, Opt. Commun. **46**, 37 (1983).

[21] D. Iracane and J. L. Ferrer, Phys. Rev. Lett. **66**, 33 (1991).

[22] I. Kimel and L. R. Elias, Phys. Rev. A **35**, 3818 (1987).

[23] *Handbook of Mathematical Functions,* Natl. Bur. Stand. Appl. Math. Ser. No. 55, edited by M. Abramowitz and I. A. Stegun (U.S. GPO, Washington, DC, 1972).